Inhibition of Monometalated Methionine Aminopeptidase: Inhibitor Discovery and Crystallographic Analysis†

Min Huang,‡ Sheng-Xue Xie,‡ Ze-Qiang Ma,‡ Qing-Qing Huang,§ Fa-Jun Nan,§ and Qi-Zhuang Ye*,‡,||

High Throughput Screening Laboratory, University of Kansas, Lawrence, Kansas 66045, Chinese National Center for Drug Screening, Shanghai Institute of Materia Medica, Chinese Academy of Sciences, Shanghai 201203, China, and Department of Biochemistry and Molecular Biology, Indiana University School of Medicine, Indianapolis, Indiana 46202

Received July 30, 2007

Two divalent metal ions are commonly seen in the active-site cavity of methionine aminopeptidase, and at least one of the metal ions is directly involved in catalysis. Although ample structural and functional information is available for dimetalated enzyme, methionine aminopeptidase likely functions as a monometalated enzyme under physiological conditions. Information on structure, as well as catalysis and inhibition, of the monometalated enzyme is lacking. By improving conditions of high-throughput screening, we identified a unique inhibitor with specificity toward the monometalated enzyme. Kinetic characterization indicates a mutual exclusivity in binding between the inhibitor and the second metal ion at the active site. This is confirmed by X-ray structure, and this inhibitor coordinates with the first metal ion and occupies the space normally occupied by the second metal ion. Kinetic and structural analyses of the inhibition by this and other inhibitors provide insight in designing effective inhibitors of methionine aminopeptidase.

Introduction

Methionine aminopeptidase[1a] is an attractive target for development of novel broad-spectrum antibiotics, because it is a protein coded by a single gene in all prokaryotes and it is essential for bacterial survival. Deletion of the MetAP gene was shown to be lethal in *Escherichia coli*[1] or *Salmonella typhimurium*.[2] In contrast, there are two genes in eukaryotic cells, coding for type I and type II MetAPs, respectively. Inhibition of human type II MetAP has been related to antiangiogenic activity of fumagillin and its analogues.[3−7] Bengamides showed potent antiproliferative activity at nanomolar concentrations in cellular assays and inhibit both types of MetAP non-discriminatively.[8] Therefore, MetAP is also a target for development of anticancer agents.

In spite of the great therapeutic potential, many potent MetAP inhibitors have not shown significant antibacterial and antiangiogenic activities.[9−12] Divalent metal ions directly participate in the removal of N-terminal methionine from nascent polypeptides by MetAP.[13] MetAP can be activated in vitro by Co(II), Mn(II), Ni(II), Zn(II), and Fe(II),[14,15] but it is not clear which of the metals is the most important inside cells. Most of the current MetAP inhibitors were discovered by using the Co(II)-form of MetAP, but it has been suggested that Fe(II) is the intrinsic metal of *E. coli* MetAP[14] and Mn(II) is the metal for human type II MetAP under physiological conditions.[16] We have shown that inhibitors have significantly different binding affinities to enzymes with different metals at the active site.[15,17] Although other factors, such as difficulty in cell-wall penetration, should be considered, it is possible that the lack of cellular efficacy for MetAP inhibitors may be partly due to a disparity between the metalloform of MetAP tested and the one that is important in cells.

Not only the identity of metal ion at the active site is in question, but the exact number of metal ions also remains to be clarified. Almost all of the available X-ray structures of MetAP have at least two metal ions, either Co(II) or Mn(II), bound at the active site with a separation of 3 Å.[17,18] However, the notion of MetAPs as dimetalated enzymes has been challenged by data from characterization of the two metal binding sites. The two sites, designated as M1 and M2, show marked differences in affinity for metal ions. Using MetAP from *E. coli*, D'souza et al. showed that dissociation constants for the tighter site were micromolar or below [K_d 300 nM, 200 nM, and 6 μM for Co(II), Fe(II), and Mn(II) respectively], but the affinity for the second metal ion was much weaker with a millimolar dissociation constant [K_d ∼2.5 mM for Co(II)].[19,20] Similarly, the affinities for metals exhibited by the MetAP from *Pyrococcus furiosus* were 50 nM, 20 nM, and 1 μM for Co(II), Fe(II), and Mn(II), respectively.[20,21] The M1 site was identified as the tighter site based on a ^{1}H NMR study.[19] Due to the weak affinity at the M2 site, the dimetalated form is less likely to exist in cells, which is supported by a spectroscopic study.[22] Recently, we showed that only one metal equivalent [Co(II) or Mn(II)] is required for full activation of *E. coli* MetAP and described the X-ray structure of *E. coli* MetAP with a transition-state inhibitor norleucine phosphonate bound as the first structure of a monometalated MetAP.[23]

Compound **1** (Figure 1) was discovered by a high-throughput screening campaign using 100 μM Mn(II) and 200 nM apoenzyme of *E. coli* MetAP, and most of MetAP is likely in dimetalated Mn(II)-form under this screening condition. This inhibitor shows not only high potency but also remarkable selectivity for MetAP activated by Mn(II).[17] A series of its derivatives, including compound **2**, were prepared and evaluated for structure−function relationships for their MetAP inhibition and metalloform selectivity.[24] During the course of our studies, we realized the importance of assay conditions for screening that should be relevant to the conditions when MetAP functions inside cells. We carried out a new screening campaign using a

† Coordinates and structure factor files for *E. coli* methionine aminopeptidase complexed to either **2** or **3** have been deposited in the Protein Data Bank under the access codes 2P9A, 2P99 and 2P98.

* Author to whom correspondence may be sent. Telephone: 317 278-0304. Fax: 317 274-4686. E-Mail: yeq@iupui.edu.

‡ University of Kansas.

§ Chinese National Center for Drug Screening.

|| Indiana University School of Medicine.

[a] MetAP, methionine aminopeptidase; AMC, 7-amino-4-methylcoumarin; MOPS, 3-(*N*-morpholino)-propanesulfonic acid.

10.1021/jm700930k CCC: $37.00 © 2007 American Chemical Society
Published on Web 10/19/2007

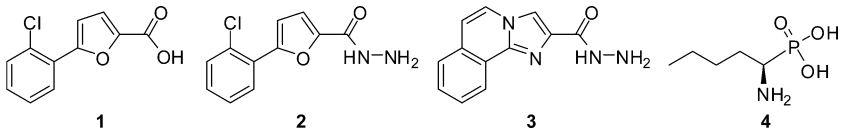

1 2 3 4

Figure 1. Structures of MetAP inhibitors. Compound **1** is a Mn(II)-form selective inhibitor described previously.[17] Compounds **2** and **3** are unique MetAP inhibitors that show preference for the monometalated form and were used for this crystallographic study. Norleucine phosphonate (**4**, NleP) is a transition-state inhibitor, and an X-ray structure of monometalated MetAP in complex with **4** was reported earlier.[23]

low concentration of metal [1 μM Co(II) and1 μM apo-MetAP] and discovered compound **3** as a unique MetAP inhibitor with specificity for monometalated MetAP. This discovery supports the notion that the monometalated form is the predominant metalloform at this low and physiologically more relevant metal concentration. Analysis of X-ray structures of *E. coli* MetAP in its monometalated and dimetalated forms in complex with **2** or **3** reveals salient features in inhibition of MetAP.

Experimental Procedures

Preparation of the Protein and Compounds. Recombinant *E. coli* MetAP was purified as an apoenzyme, and it was metal-free according to metal analysis.[15] A chemical library of 98,208 small organic molecules used for screening was purchased from ChemBridge and ChemDiv (both at San Diego, CA), and these compounds were selected from vendors' much larger compound collections for structural diversity and drug-like properties. Reactive, unstable, and potentially toxic compounds were eliminated in the selection process. All compounds have molecular weight between 150 and 480 and calculated LogP (cLogP) below 5. Substrate Met-AMC, a methionine derivatized with 7-amino-4-methylcoumarin (AMC), was purchased from Bachem Bioscience (King of Prussia, PA). Compound **2** was synthesized in our laboratory.[24] Compound **3** was purchased from ChemBridge and characterized by ^{1}H and ^{13}C NMR and high-resolution mass spectrometry.

MetAP Activity Assay. Enzymatic activity of MetAP was monitored by a fluorescence assay using Met-AMC as a fluorogenic substrate.[15,25] Hydrolysis of the amide bond in Met-AMC releases the fluorescent AMC (λ_{ex} 360 nm, λ_{em} 460 nm). The assay was performed on 384-well flat-bottom polystyrene microplates on a SpectraMax Gemini XS microplate fluorescence reader (Molecular Devices, Sunnyvale, CA). The assay mixture (80 μL final volume) typically contains 50 mM MOPS (pH 7.0), 1 μM apo-MetAP, 200 μM Met-AMC, and metal ions ($CoCl_2$ or $MnCl_2$). The metal concentration is typically 100 μM, and for the metal concentration dependence experiment, the concentration of $MnCl_2$ varied from 5 to 200 μM.

High-Throughput Screening for MetAP Inhibitors. A total of 98,208 screening compounds were distributed on 279 384-well plates. Each plate had 352 wells for 352 compounds and 32 wells for positive and negative controls. The negative control wells contained no screening compounds, and the positive control wells contained no screening compounds and no apoenzyme. Assay mixture (80 μL final volume) consisted of 50 mM MOPS (pH 7.0), 200 μM Met-AMC, 1 μM apo-MetAP, 1 μM $CoCl_2$, and 6.25 μg/mL screening compound. Screening was carried out by monitoring fluorescence on an Envision multilabel plate reader (Perkin-Elmer, Wellesley, MA) with filters at 355 nm for excitation and 460 nm for emission. Screening using these assay conditions and these compounds generated high-quality data with z' factors[26] between 0.57 and 0.92 and their average at 0.80. Screening hits were ranked according to their potencies (percent inhibition), and the top ranked hits were selected for confirmation of inhibitory activity by determining their IC_{50} values using six compound concentrations. Liquid handling for hit-picking and serial dilutions was carried out on a Biomek FX liquid handling workstation (Beckman Coulter, Fullerton, CA) and a Precision 2000 automated microplate pipetting system (BioTek Instruments, Winooski, VT).

Crystallization Conditions. Initial crystallization conditions were determined using Crystal Screen and Index HT kits in 96-well sitting-drop plates (Hampton Research, Aliso Viejo, CA) at room temperature. Final crystals of the enzyme−inhibitor complexes were obtained independently by the hanging-drop vapor-diffusion method at 18−20 °C. Inhibitors (200 mM in DMSO) were added to concentrated apoenzyme (12 mg/mL, 0.4 mM) in 10 mM MOPS (pH 7.0). Hanging drops contained 3 μL of protein solution mixed with 3 μL of reservoir solution. The reservoir solution consisted of 10−15% PEG 20 000, 0.1 M MES (pH 6.5) and 0.2 mM or 0.8 mM $MnCl_2$. The concentration ratio of inhibitor/apoenzyme was 10:1 for either **2** or **3**, and that of metal/apoenzyme was 0.5:1 or 2:1.

Data Collection and Structural Refinement. Collection of diffraction data was assisted by personnel at Protein Structure Laboratory at University of Kansas. Data were collected on an R-Axis IV imaging plate detector with a Rigaku rotating anode generator operated at 50 kV and 100 mA. Images were recorded over 180° in 0.5° increments at 100 K. The raw reflection data were processed using MOSFLM and merged and scaled using SCALA in CCP4 with CCP4i interface.[27] Crystals of the monometalated enzyme were in the same crystal form as those of the dimetalated enzyme, and cell analysis of the data indicated only one molecule of the enzyme per asymmetric unit in all three cases. The coordinates of our previously solved structure of *E. coli* MetAP (PDB code 1XNZ) with ligand, metal ions, and water molecules removed were used as the search model for molecular replacement using MOLREP in CCP4. Crystallographic refinement was performed with CNS.[28] The refinement was monitored using 10% of the reflections set aside for free *R* factor analysis throughout the whole refinement process. Initial refinement started with simulated annealing with a starting temperature at 4000 and 25 K drop in temperature per cycle. The models were refined with iterative cycles of individual *B* factor refinement, positional refinement, and manual model building using WinCoot.[29] Mn(II) atoms were not included in initial refinement procedure to reduce model bias in phases and were then added to the model to the center of the peak in the Mn(II)-omitted $F_{obs} - F_{calc}$ electron density map. The ligand and water molecules were added when the electron densities shown in $2F_{obs} - F_{calc}$ and $F_{obs} - F_{calc}$ maps for their placement were unequivocal. The final $2F_{obs} - F_{calc}$ maps showed clear electron density for most of the atoms except for a few side chains at molecular surface. The final models for all of the structures were analyzed using the program PROCHECK,[30] and all have 99.6% of residues in the allowed region of their respective Ramachandran plots. The atomic coordinates and structure factors for the structures have been deposited in the Protein Data Bank. All drawings for protein structures in figures were generated using PYMOL.[31] Statistical parameters in data collection and structural refinement are shown in Table 1.

Results and Discussion

Discovery of Compound 3 as an Inhibitor of Monometalated MetAP by High-Throughput Screening. MetAP enzymes are maximally activated by divalent metals at high micromolar concentrations,[15] and most MetAP inhibitors were identified with enzyme assays using high micromolar concentrations of the metals, commonly Co(II). Before our recent publication of a monometalated MetAP structure,[23] all MetAP X-ray structures showed two or more metal ions at the active-site cavity,[18] possibly due to excess amounts of metal ion used during crystallization. Similarly, high metal concentrations in assays favor formation of the dimetalated form during screening

Table 1. X-ray Data Collection and Refinement Statistics

PDB code	2P9A	2P99	2P98
ligand	**2**	**2**	**3**
metal	2 Mn	1 Mn	1 Mn
Cell Parameters			
space group	$P2_1$	$P2_1$	$P2_1$
a (Å)	38.0	38.3	38.2
b (Å)	60.6	61.7	60.3
c (Å)	50.5	50.6	50.6
β (deg)	104.8	105.4	104.6
X-ray Data Collection			
resolution range (Å)			
overall	18.9−1.6	19.1−1.8	19.8−1.7
outer shell	1.7−1.6	1.9−1.8	1.8−1.7
collected reflections	103,700	76,584	87,470
unique reflections	28,157	20,276	23,375
completeness (%)[a]	96.3 (93.5)	97.9 (95.9)	95.5 (92.7)
I/σ (*I*)[a]	24.7 (4.5)	18.2 (3.1)	22.6 (4.2)
R_{merge} (%)[a]	3.3 (22.0)	5.1 (33.7)	3.8 (24.9)
Refinement Statistics			
R (%)	20.6	22.6	20.7
R_{free} (%)	23.1	26.3	23.8
rmsd bonds (Å)	0.005	0.006	0.005
rmsd angles (deg)	1.29	1.36	1.34
no. of solvent molecules	179	152	158
<B> enzyme (Å^2)	19.6	25.8	22.7
<B> inhibitor (Å^2)	25.6	28.8	26.6
<B> water (Å^2)	28.5	32.0	30.2

[a] Numbers given in parentheses correspond to the outer shell of data.

Table 2. Inhibition[a] of MetAP by Compounds **1**−**3** at Different Metal Concentrations

compd	Mn at 100 μM	Mn at 5 μM	Co at 100 μM	Co at 1 μM	Ni at 10 μM	Fe at 6 μM
1	0.51	0.78	138	>200	141	116
2	6.56	1.16	77.1	n.t.[b]	5.78	58.0
3	4.31	0.64	27.8	2.44	6.15	17.4

[a] IC_{50} values in μM. [b] Not tested.

for MetAP inhibitors. In light of the evidence that only one of the two metal ions at the active site is tightly bound,[19−21] it is likely that the physiologically relevant form of MetAPs possess a single metal ion rather than two. To discover compounds as inhibitors of the monometalated form, we modified the assay conditions so that the Co(II) concentration was lowered to 1 μM, instead of 100 μM used previously,[10,17] to match the concentration of apoenzyme (1 μM). Activation of apo-MetAP by divalent metal ions is instantaneous,[15] so that the screening was performed by mixing Co(II), apoenzyme, and the screening compound, and the mixture was incubated at room temperature for 90 min. Then, hydrolysis of the substrate Met-AMC was determined by measuring fluorescence of AMC generated.[15,25] Although the chemical library used for the screening contains a large number of small organic compounds with diverse structures, this screening identified compound **3** among the top 50 hits. Its unique inhibitory activity, as well as its structural similarities to compounds **1** and **2**, caught our attention, and its further characterization was pursued.

Inhibition of MetAP with Different Divalent Metals by 3 in Comparison to 1 and 2. Compound **1** was discovered by high-throughput screening, and it shows high potency and great selectivity for *E. coli* MetAP activated by Mn(II)[17] (Table 2). Compound **2** was among several derivatives of **1** made to study the structure−function relationships, and although it still has good inhibitory activity for the Mn(II)-form, it is much less selective[24] (Table 2). The metal concentrations used in the assays to obtain these IC_{50} values are relatively high [Mn(II), 100 μM; Co(II), 100 μM; Ni(II), 10 μM; Fe(II), 6 μM], and the enzyme likely existed in a mixture of both monometalated and dimetalated forms at different ratios. Under the same assay conditions, compound **3** showed good inhibitory activities on the different metalloforms but was also much less selective [IC_{50} 4.31, 27.8, 6.15, and 17.4 μM for Mn(II)-, Co(II)-, Ni(II)-, and Fe(II)-forms, respectively] (Table 2). The common structural feature shared by compounds **2** and **3** is the carbonylhydrazide group, and it may contribute to their much reduced metalloform selectivity.

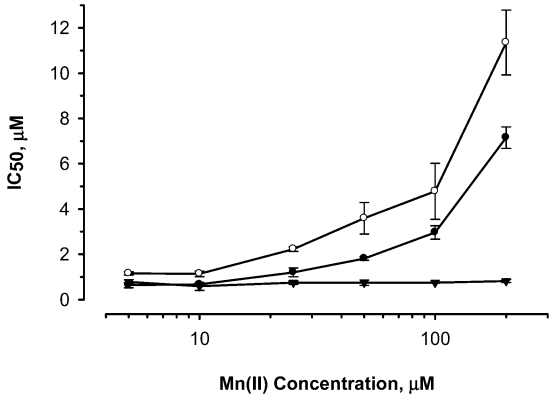

Figure 2. Effect of Mn(II) concentration on inhibitory activity of compounds **1** (▼), **2** (○), and **3** (●). Compounds **1**, **2**, and **3** were also tested under different concentrations of Co(II), and the same trend was observed.

Dependence of Inhibition of MetAP by 2 and 3 on Metal Ion Concentration. It is interesting to note that compound **3**, as a screening hit, has low micromolar potency (IC_{50}, 2.44 μM) when its activity was confirmed with 1 μM apo-MetAP and 1 μM Co(II), and the potency is significantly decreased (IC_{50}, 27.8 μM) when 100 μM Co(II) was used in the assay (Table 2). Previously, we noticed that the potency of compound **2** was also affected by metal concentration [IC_{50}, 1.16 or 6.56 μM, at 5 μM or 100 μM Mn(II), respectively]. When compounds **2** and **3** were tested at more metal concentrations, the trend becomes clear. Increase of the metal concentration, either Co(II) or Mn(II), greatly decreases their inhibitory activity (Figure 2). Interestingly, the inhibitory activity of **1** is not affected by metal concentrations. The binding mode of **1** was revealed by a dimetalated X-ray structure, and the carboxylate of **1** directly interacts with the metal ions at the active site. Compounds **2** and **3** are structurally similar to **1**. Similarity between **1** and **2** is apparent, and **3** has both six-membered (phenyl) and five-membered (imidazole) rings embedded. If **2** and **3** bind to MetAP with their six-membered and five-membered rings occupying the similar spaces, part of the carbonylhydrazide moiety will protrude into the site for M2. Potential competition for binding between the second metal ion and the inhibitor could explain the inhibition that is affected by metal concentrations.

Crystallization of the Complexes of *E. coli* MetAP with either 2 or 3. In parallel with the kinetic studies, we solved a crystal structure of the complex between compound **2** and *E. coli* MetAP in a dimetalated form to 1.6 Å resolution (Table 1). To our surprise, although **2** still binds within the active-site cavity, it occupies a unique orientation and does not interact with the two Mn(II) ions in the active site (Figures 3B and 4A). Previously solved structure of **1** with *E. coli* MetAP shows that the inhibitor coordinates with both Mn(II) ions and is a bidentate ligand to the Mn(II) ion at M1 site and a monodentate ligand to the Mn(II) ion at M2 site (Figure 3A).[17] These two dimetalated Mn(II)-form structures support our hypothesis that changing the carboxyl moiety in **1** to a carbonylhydrazide moiety in **2** puts the terminal amino group of hydrazide in a position to compete for space with the M2 metal ion. An excess amount

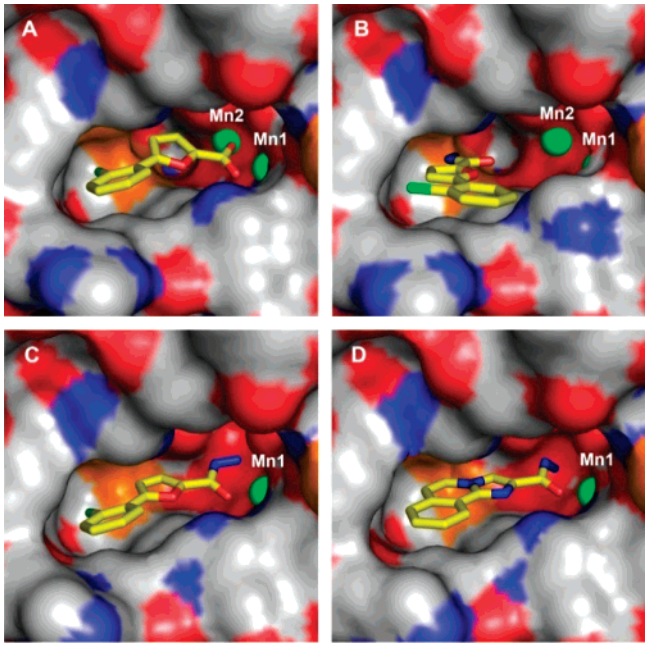

Figure 3. Close-up views of the inhibitors **1** (A), **2** (B and C), and **3** (D) bound at the dimetalated (A and B) and monometalated (C and D) sites. The inhibitors are shown as sticks and colored carbon yellow, oxygen red, nitrogen blue, and chlorine green. The active-site pocket is shown as solid surface (carbon gray, oxygen red, nitrogen blue, and sulfur orange). The Mn(II) ions are shown as green spheres and indicated as Mn1 and Mn2.

of metal ion used during crystallization led to the formation of a dimetalated enzyme and forced compound **2** to bind in the orientation observed in Figures 3B and 4A. To obtain an *E. coli* MetAP structure in complex with its inhibitor that more accurately reflects the likely situation in cells, we attempted to obtain crystals of *E. coli* MetAP in complex with either **2** or **3** under the conditions with limiting amounts of Mn(II) present during crystallization (ratio of metal/apoenzyme 0.5:1 or 2:1). The crystals generated through this approach consistently produced high-quality diffraction data for structural solution of the monometalated MetAP with resolutions of 1.7 and 1.8 Å, respectively (Table 1). It is interesting to note that MetAP was crystallized with **2** as a dimetalated form when the ratio of metal/apoenzyme was 2:1 and as a monometalated form when the ratio was 0.5:1. However, MetAP was crystallized with **3** as a monometalated form under both conditions. This observation is consistent with the affinity of **2** and **3** to MetAP as indicated by their IC_{50} values. Compound **3** is a more potent inhibitor than **2**.

Structure of Dimetalated MetAP with 2 Bound. The overall structure of this dimetalated Mn(II)-form is typical of all dimetalated forms of MetAPs solved to date (Figures 3B and 4A).[5,32−34] The two Mn(II) ions occupy the M1 and M2 sites in which one water molecule (or hydroxide) bridges the two metal ions. Mn1 exhibits nearly trigonal bipyrimidal geometry, and Mn2 exhibits octahedral coordination, with the sixth ligand provided by a water molecule commonly seen in other structures. Compound **2** is situated at the mouth of the active-site cavity with a nearly coplanar arrangement of the two aromatic rings (dihedral angle 4.0°), and the molecule does not directly coordinate to either of the Mn(II) ions. The near coplanar conformation is unusual because compound **1** is bound with a dihedral angle of 41.5° between the adjacent rings[17] and a 2,5-dichloro analogue of **1** has a dihedral angle of 32.0°.[34] The energetically unfavorable near-coplanar conformation for **2** observed here, in combination with the lack of direct metal ion coordination, explains the reduced inhibitory activity of **2** at high Mn(II) concentrations.

Structure of Monometalated MetAP with 2 Bound. The monometalated structure solved at low metal concentration (metal/apo-MetAP ratio 0.5:1) shows clearly only a single Mn(II) ion bound in the active site, located at the M1 site (Figures 3C and 4B). In contrast to the dimetalated structure, compound **2** now coordinates in a bidentate manner to the Mn(II) ion using its carbonyl oxygen and the terminal amino nitrogen, with the heteroatom−metal distances at 2.3 and 2.4 Å, respectively. As predicted, the binding mode of **2** in the monometalated structure is similar to that of **1** in the dimetalated structure. Consistent with the kinetic data above, the terminal amino group indeed protrudes into the space normally occupied by Mn2 and prevents its binding. Mn1 is coordinated in an octahedral manner. Similar to that observed for compound **1**, the dihedral angle between the phenyl and furan rings produces a noncoplanar conformation (20.5°). However, although the carboxyl group (O−C═O) in **1** is coplanar with the furan ring, the plane of the carbonylhydrazide (N−C═O) in **2** rotates away from a coplanar conformation with the furan ring and exhibits a dihedral angle (O−C−C═O) of 23.0°. Finally, in the absence of Mn2, D97 rotates about the Cβ−Cγ axis, similar to what we observed in the previous monometalated structure of MetAP,[23] indicating that this conformation for D97 is closer to its low-energy conformation in the absence of the unnatural influence by Mn2.

Structure of Monometalated MetAP with 3 Bound. Crystals grown at high and low metal concentrations (metal to apo-MetAP ratios 2:1 and 0.5:1) produced the same monometalated structure (Figures 3D and 4C). Compound **3** binds to monometalated MetAP in the same mode as **2** and coordinates with the sole metal at M1 site (Mn1). However, the interaction between the carbonylhydrazide and the metal is very different between **2** and **3**, and **3** is a monodentate ligand to Mn1. Instead of forming a heteroatom−metal bond with Mn1, the terminal amino group of the carbonylhydrazide moves away from Mn1 and extends into the center of the space commonly occupied by Mn2. The distance from the amino nitrogen to Mn1 is 3.0 Å, while the distance between Mn1 and Mn2 in the dimetalated structure with **2** is 3.3 Å. The amino group in carbonylhydrazide is likely to be deprotonated under the crystallization conditions due to its estimated pK_a of 3−4[35,36] being more than 2.5 units below the pH of the crystallization solution. However, the nitrogen of the amino group is close enough to the carboxyl oxygens of D97 (2.5 and 3.0 Å), D108 (2.4 Å), and E235 (2.5 Å) to form hydrogen bonding. The plane (N−C═O) of the carbonylhydrazide in **3** is also not coplanar with the tricyclic backbone, exhibiting a dihedral angle (O−C−C═O) of 22.2°.

Comparison among Monometalated and Dimetalated Structures. Our previous monometalated MetAP structure in complex with norleucine phosphonate **4**[23] was also obtained in the presence of limiting metal concentrations during crystallization. In contrast to **2** and **3**, inhibitor **4** has no functional group to compete for the second metal site. An alignment of all three available monometalated MetAP structures reveals some features that may be important for binding substrate and inhibitor effectively (Figure 5A). Noticeably, the side chains of D97, H79, and W221 move in response to the characteristics of the ligand present. D97 was proposed as a crucial residue to bind the terminal amino group of the substrate,[23,37] and it forms hydrogen bonds directly or indirectly through water molecules with the inhibitors by rotating around its Cβ−Cγ axis. H79 was suggested to play an essential role in catalysis, and its mobility may be required for its role in delivering a proton and for

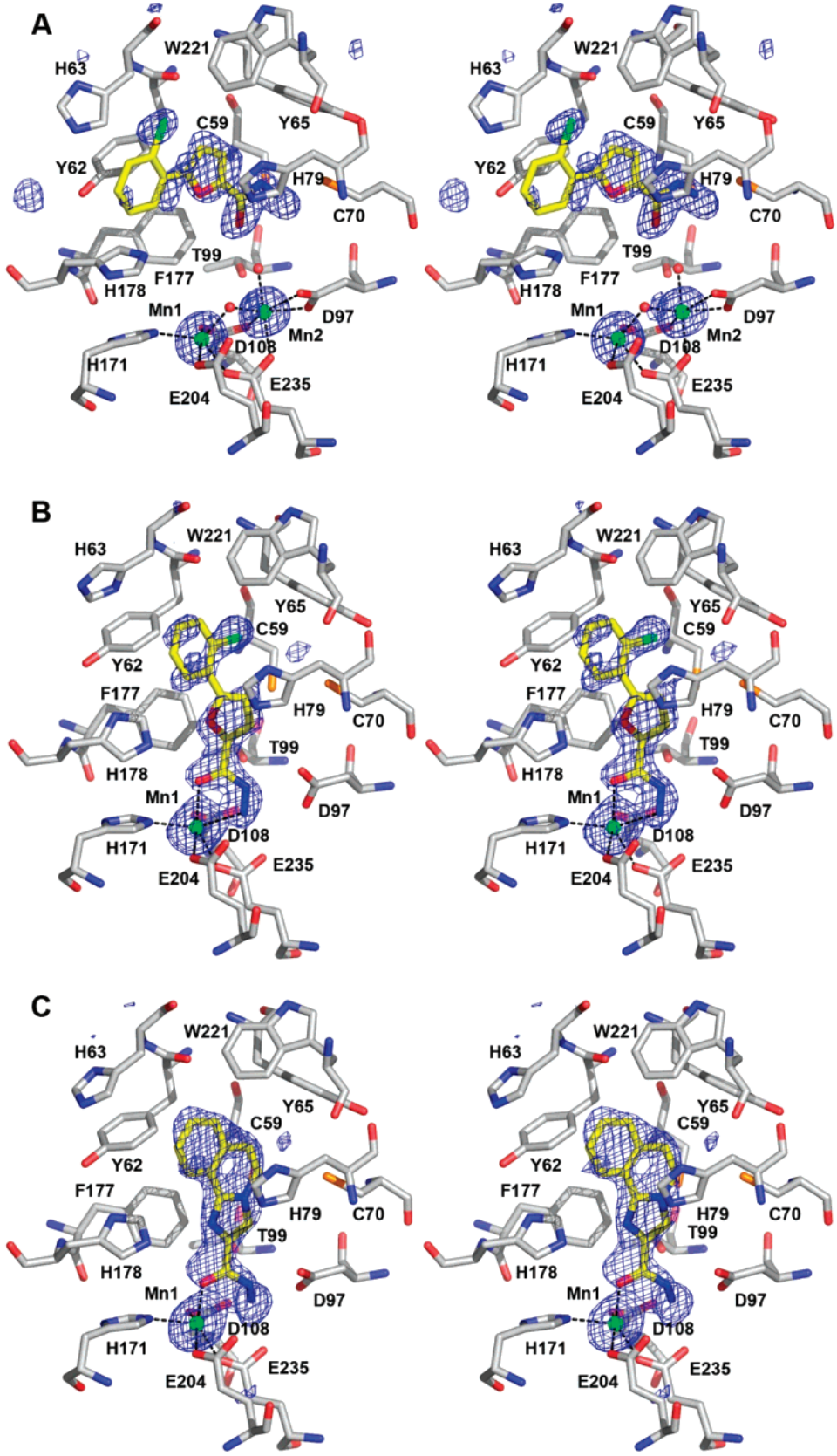

Figure 4. Binding modes of **2** with dimetalated (A) or monometalated (B) MetAP and of **3** with monometalated MetAP (C). Shown here are stereoviews of partial structures at the ligand binding site. Color scheme: carbon gray (protein residues) or yellow (inhibitor), nitrogen blue, oxygen red, sulfur orange, and chlorine green. Mn(II) ions are shown as green spheres, and water molecules as smaller red spheres. $F_{obs} - F_{calc}$ omit maps (inhibitor and metal ions were not included in the model) are shown superimposed on the refined structures as blue meshes contoured at 3.5σ.

releasing the reaction product. W221 also showed noticeable movement to adapt to different bound inhibitors. Inhibitor **4** is known to mimic the methionine residue in substrate with its norleucine side chain and binds at the S1 site,[38] and inhibitors **2** and **3** generally trace the norleucine side chain with their aromatic moieties and also bind at the S1 site. Superposition of

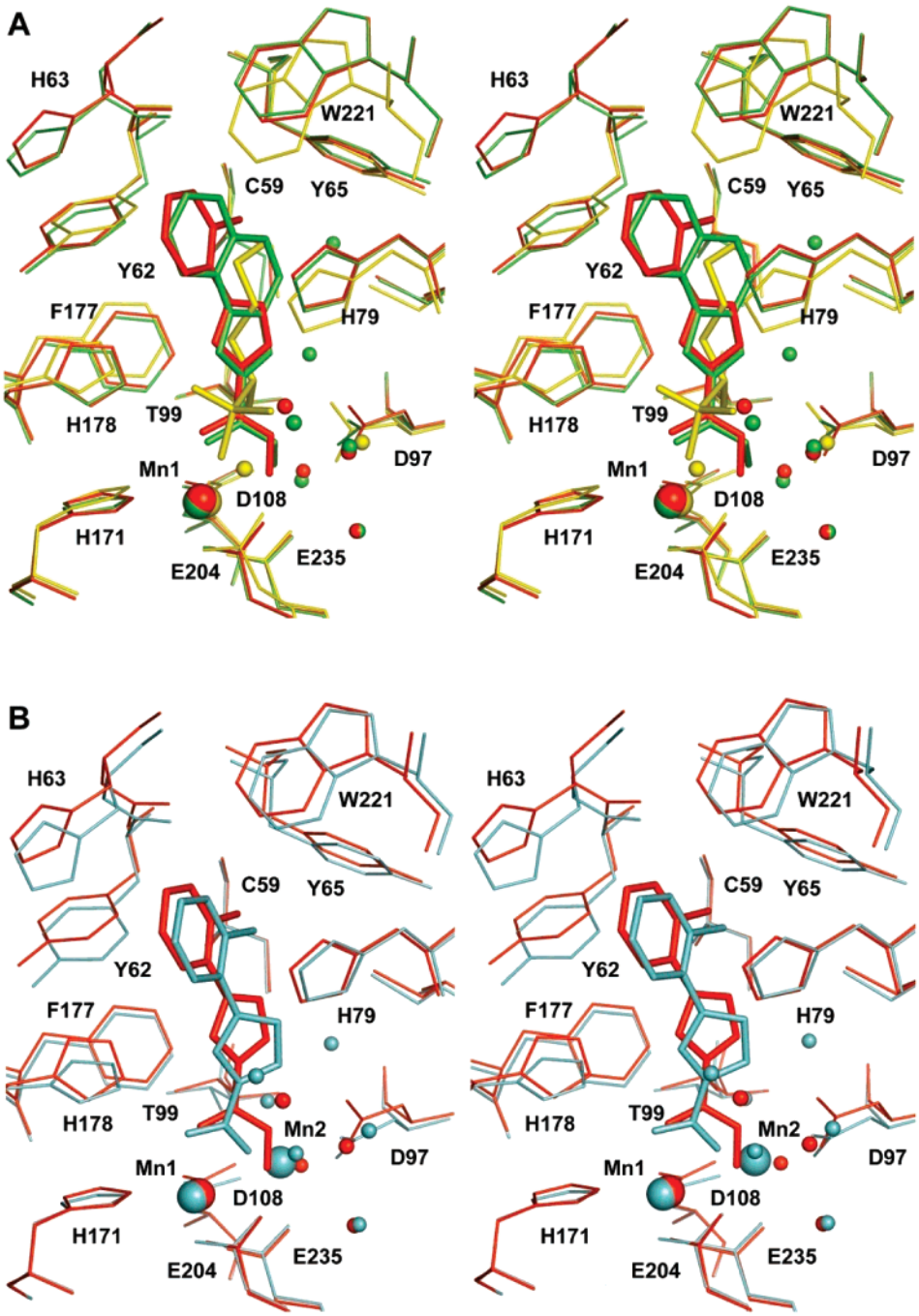

Figure 5. Comparison among monometalated MetAP structures (A) and between monometalated and dimetalated structures (B). The structures used for superposition are complexes with **2** (red), **3** (green), and **4** (yellow) in A, and **2** (red) and **1** (cyan) in B. The inhibitors are shown in thick sticks, and the residues at the active site in thin sticks. Bigger spheres are Mn(II) ions, and smaller spheres are water molecules.

the structures with **2** and **3** bound in the monometalated forms of MetAP shows that the furan ring in **2** and the imidazo[2,1-*a*]isoquinoline in **3** are coplanar, and the furan ring in **2** occupies the position similar to that of the imidazole moiety in **3**.

The structure of *E. coli* MetAP in complex with **1** is typical of dimetalated forms of MetAP, and an overlay with the monometalated form of MetAP in complex with **2** shows the differences in the presence and absence of the second metal ion (Figure 5B). The most significant difference is the position of residue D97. In all dimetalated structures, it functions as a bidentate ligand for M2. In the absence of M2, its movement is no longer restricted, and it adapts to interact with the bound inhibitors.

Design of MetAP Inhibitors for Efficacy in Cells. Structural and kinetic evidence supports the monometalated form of MetAP as the relevant metalloform in cells. Discovery and characterization of compound **3** as a unique specific inhibitor of this monometalated form provide further evidence that the monometalated form is the predominant metalloform when metal is present at low concentration and inhibitors with such unique properties can be identified by high-throughput screening. For efficacy in cells, MetAP inhibitors need to inhibit the physiologically relevant metalloform effectively. Compounds **2** and **3** inhibit the monometalated MetAP enzyme at low micromolar potency, and they are promising leads for further development. Initial testing showed that their inhibition of *E. coli* growth was

weak, and the lack of activity on *E. coli* cells could be due to many reasons including insufficient potency and poor permeability into the cells. Structural improvement of **2** and **3** is currently underway to increase their potency on MetAP enzyme and their cellular activity.

Structures of dimetalated and trimetalated MetAP in complex with non-peptidic inhibitors are abundant in literature.[11,12,34,39,40] When a high metal concentration is used in inhibitor screening, the condition favors formation of dimetalated MetAP, and the screening tends to identify inhibitors that require extra metal ions for affinity. However, in the absence of a substrate or an inhibitor, the affinity of the second metal ion to MetAP is low,[19,20] and the affinity of the third metal ion is probably even lower because no structure of a trimetalated MetAP has been obtained without an inhibitor present. Considering that the free metal concentrations in cells are low,[41] many of these inhibitors may not have potency in cells. Although inhibitors that inhibit only the monometalated MetAP are not required, to be therapeutically useful, potent inhibitors of the monometalated form are desirable. All MetAP inhibitors should function at physiologically relevant metal concentrations.

Acknowledgment. We thank Profs. Gunda Georg and Robert Hanzlik for their intellectual support during this study and Dr. Wei-Jun Huang for his assistance in X-ray data collection. We also thank Profs. Thomas Hurley and Zhong-Yin Zhang for their critical reading of the manuscript and helpful suggestions. This research was supported by National Institutes of Health Grants R01 AI065898, P20 RR015563, and P20 RR016475 (to Q.-Z.Y.). The High Throughput Screening Laboratory and the Protein Structure Laboratory were supported by National Institutes of Health Grants P20 RR015563 and P20 RR017708 from the Centers of Biomedical Research Excellence program of the National Center for Research Resources, the University of Kansas, and the Kansas Technology Enterprise Corporation.

References

(1) Chang, S. Y.; McGary, E. C.; Chang, S. Methionine aminopeptidase gene of Escherichia coli is essential for cell growth. *J. Bacteriol.* **1989**, *171*, 4071−4072.
(2) Miller, C. G.; Kukral, A. M.; Miller, J. L.; Movva, N. R. pepM is an essential gene in Salmonella typhimurium. *J. Bacteriol.* **1989**, *171*, 5215−5217.
(3) Griffith, E. C.; Su, Z.; Niwayama, S.; Ramsay, C. A.; Chang, Y. H.; Liu, J. O. Molecular recognition of angiogenesis inhibitors fumagillin and ovalicin by methionine aminopeptidase 2. *Proc. Natl. Acad. Sci. U.S.A.* **1998**, *95*, 15183−15188.
(4) Griffith, E. C.; Su, Z.; Turk, B. E.; Chen, S.; Chang, Y. H.; Wu, Z.; Biemann, K.; Liu, J. O. Methionine aminopeptidase (type 2) is the common target for angiogenesis inhibitors AGM-1470 and ovalicin. *Chem Biol* **1997**, *4*, 461−471.
(5) Liu, S.; Widom, J.; Kemp, C. W.; Crews, C. M.; Clardy, J. Structure of human methionine aminopeptidase-2 complexed with fumagillin. *Science* **1998**, *282*, 1324−1327.
(6) Turk, B. E.; Griffith, E. C.; Wolf, S.; Biemann, K.; Chang, Y. H.; Liu, J. O. Selective inhibition of amino-terminal methionine processing by TNP-470 and ovalicin in endothelial cells. *Chem. Biol.* **1999**, *6*, 823−833.
(7) Turk, B. E.; Su, Z.; Liu, J. O. Synthetic analogues of TNP-470 and ovalicin reveal a common molecular basis for inhibition of angiogenesis and immunosuppression. *Bioorg. Med. Chem.* **1998**, *6*, 1163−1169.
(8) Towbin, H.; Bair, K. W.; DeCaprio, J. A.; Eck, M. J.; Kim, S.; Kinder, F. R.; Morollo, A.; Mueller, D. R.; Schindler, P.; Song, H. K.; van Oostrum, J.; Versace, R. W.; Voshol, H.; Wood, J.; Zabludoff, S.; Phillips, P. E. Proteomics-based target identification: bengamides as a new class of methionine aminopeptidase inhibitors. *J. Biol. Chem.* **2003**, *278*, 52964−52971.
(9) Garrabrant, T.; Tuman, R. W.; Ludovici, D.; Tominovich, R.; Simoneaux, R. L.; Galemmo, R. A., Jr.; Johnson, D. L. Small molecule inhibitors of methionine aminopeptidase type 2 (MetAP-2) fail to inhibit endothelial cell proliferation or formation of microvessels from rat aortic rings in vitro. *Angiogenesis* **2004**, *7*, 91−96.
(10) Luo, Q. L.; Li, J. Y.; Liu, Z. Y.; Chen, L. L.; Li, J.; Qian, Z.; Shen, Q.; Li, Y.; Lushington, G. H.; Ye, Q. Z.; Nan, F. J. Discovery and structural modification of inhibitors of methionine aminopeptidases from Escherichia coli and Saccharomyces cerevisiae. *J. Med. Chem.* **2003**, *46*, 2631−2640.
(11) Oefner, C.; Douangamath, A.; D'Arcy, A.; Hafeli, S.; Mareque, D.; Mac, Sweeney, A.; Padilla, J.; Pierau, S.; Schulz, H.; Thormann, M.; Wadman, S.; Dale, G. E. The 1.15A crystal structure of the Staphylococcus aureus methionyl-aminopeptidase and complexes with triazole based inhibitors. *J. Mol. Biol.* **2003**, *332*, 13−21.
(12) Schiffmann, R.; Heine, A.; Klebe, G.; Klein, C. D. Metal ions as cofactors for the binding of inhibitors to methionine aminopeptidase: A critical view of the relevance of in vitro metalloenzyme assays. *Angew. Chem., Int. Ed.* **2005**, *44*, 3620−3623.
(13) Lowther, W. T.; Matthews, B. W. Metalloaminopeptidases: common functional themes in disparate structural surroundings. *Chem. Rev.* **2002**, *102*, 4581−4608.
(14) D'Souza, V. M.; Holz, R. C. The methionyl aminopeptidase from Escherichia coli can function as an iron(II) enzyme. *Biochemistry* **1999**, *38*, 11079−11085.
(15) Li, J. Y.; Chen, L. L.; Cui, Y. M.; Luo, Q. L.; Li, J.; Nan, F. J.; Ye, Q. Z. Specificity for inhibitors of metal-substituted methionine aminopeptidase. *Biochem. Biophys. Res. Commun.* **2003**, *307*, 172−179.
(16) Wang, J.; Sheppard, G. S.; Lou, P.; Kawai, M.; Park, C.; Egan, D. A.; Schneider, A.; Bouska, J.; Lesniewski, R.; Henkin, J. Physiologically relevant metal cofactor for methionine aminopeptidase-2 is manganese. *Biochemistry* **2003**, *42*, 5035−5042.
(17) Ye, Q. Z.; Xie, S. X.; Huang, M.; Huang, W. J.; Lu, J. P.; Ma, Z. Q. Metalloform-selective inhibitors of escherichia coli methionine aminopeptidase and X-ray structure of a Mn(II)-form enzyme complexed with an inhibitor. *J. Am. Chem. Soc.* **2004**, *126*, 13940−13941.
(18) Lowther, W. T.; Matthews, B. W. Structure and function of the methionine aminopeptidases. *Biochim. Biophys. Acta* **2000**, *1477*, 157−167.
(19) D'Souza, V. M.; Bennett, B.; Copik, A. J.; Holz, R. C. Divalent metal binding properties of the methionyl aminopeptidase from Escherichia coli. *Biochemistry* **2000**, *39*, 3817−3826.
(20) D'Souza, V. M.; Swierczek, S. I.; Cosper, N. J.; Meng, L.; Ruebush, S.; Copik, A. J.; Scott, R. A.; Holz, R. C. Kinetic and structural characterization of manganese(II)-loaded methionyl aminopeptidases. *Biochemistry* **2002**, *41*, 13096−13105.
(21) Meng, L.; Ruebush, S.; D'Souza, V, M.; Copik, A. J.; Tsunasawa, S.; Holz, R. C. Overexpression and divalent metal binding properties of the methionyl aminopeptidase from Pyrococcus furiosus. *Biochemistry* **2002**, *41*, 7199−7208.
(22) Cosper, N. J.; D'Souza, V, M.; Scott, R. A.; Holz, R. C. Structural evidence that the methionyl aminopeptidase from Escherichia coli is a mononuclear metalloprotease. *Biochemistry* **2001**, *40*, 13302−13309.
(23) Ye, Q. Z.; Xie, S. X.; Ma, Z. Q.; Huang, M.; Hanzlik, R. P. Structural basis of catalysis by monometalated methionine aminopeptidase. *Proc. Natl. Acad. Sci. U.S.A.* **2006**, *103*, 9470−9475.
(24) Huang, Q. Q.; Huang, M.; Nan, F. J.; Ye, Q. Z. Metalloform-selective inhibition: Synthesis and structure-activity analysis of Mn(II)-form-selective inhibitors of Escherichia coli methionine aminopeptidase. *Bioorg. Med. Chem. Lett.* **2005**, *15*, 5386−5391.
(25) Yang, G.; Kirkpatrick, R. B.; Ho, T.; Zhang, G. F.; Liang, P. H.; Johanson, K. O.; Casper, D. J.; Doyle, M. L.; Marino, J. P., Jr.; Thompson, S. K.; Chen, W.; Tew, D. G.; Meek, T. D. Steady-state kinetic characterization of substrates and metal-ion specificities of the full-length and N-terminally truncated recombinant human methionine aminopeptidases (type 2). *Biochemistry* **2001**, *40*, 10645−10654.
(26) Zhang, J. H.; Chung, T. D.; Oldenburg, K. R. A simple statistical parameter for use in evaluation and validation of high throughput screening assays. *J. Biomol. Screening* **1999**, *4*, 67−73.
(27) Collaborative Computational Project Number 4. The CCP4 Suite: Programs for Protein Crystallography. *Acta Crystallogr.* **1994**, *D50*, 760−763.
(28) Brunger, A. T.; Adams, P. D.; Clore, G. M.; DeLano, W. L.; Gros, P.; Grosse-Kunstleve, R. W.; Jiang, J. S.; Kuszewski, J.; Nilges, M.; Pannu, N. S.; Read, R. J.; Rice, L. M.; Simonson, T.; Warren, G. L. Crystallography & NMR system: A new software suite for macromolecular structure determination. *Acta Crystallogr., Sect. D* **1998**, *54* (Pt 5), 905−921.

(29) Emsley, P.; Cowtan, K. Coot: model-building tools for molecular graphics. *Acta Crystallogr., Sect. D* **2004**, *60*, 2126−2132.
(30) Laskowski, R. A.; MacArthur, M. W.; Moss, D. S.; Thornton, J. M. PROCHECK: a program to check the stereochemical quality of protein structures. *J. Appl. Crystallogr.* **1993**, *26*, 283−291.
(31) DeLano, W. L. The PyMOL Molecular Graphics System. on World Wide Web; http://www.pymol.org, 2002.
(32) Copik, A. J.; Waterson, S.; Swierczek, S. I.; Bennett, B.; Holz, R. C. Both nucleophile and substrate bind to the catalytic Fe(II)-center in the type-II methionyl aminopeptidase from Pyrococcus furiosus. *Inorg. Chem.* **2005**, *44*, 1160−1162.
(33) Roderick, S. L.; Matthews, B. W. Structure of the cobalt-dependent methionine aminopeptidase from Escherichia coli: a new type of proteolytic enzyme. *Biochemistry* **1993**, *32*, 3907−3912.
(34) Xie, S. X.; Huang, W. J.; Ma, Z. Q.; Huang, M.; Hanzlik, R. P.; Ye, Q. Z. Structural analysis of metalloform-selective inhibition of methionine aminopeptidase. *Acta Crystallogr., Sect. D* **2006**, *62*, 425−432.
(35) Lindegren, C. R.; Niemann, C. The apparent ionization constants of acethydrazide and glycylhydrazide. *J. Am. Chem. Soc.* **1949**, *71*, 1504−1504.
(36) Raddatz, S.; Mueller-Ibeler, J.; Kluge, J.; Wass, L.; Burdinski, G.; Havens, J. R.; Onofrey, T. J.; Wang, D.; Schweitzer, M. Hydrazide oligonucleotides: new chemical modification for chip array attachment and conjugation. *Nucleic Acids Res.* **2002**, *30*, 4793−4802.
(37) Copik, A. J.; Swierczek, S. I.; Lowther, W. T.; D'Souza, V, M.; Matthews, B. W.; Holz, R. C. Kinetic and spectroscopic characterization of the H178A methionyl aminopeptidase from Escherichia coli. *Biochemistry* **2003**, *42*, 6283−6292.
(38) Lowther, W. T.; Zhang, Y.; Sampson, P. B.; Honek, J. F.; Matthews, B. W. Insights into the mechanism of Escherichia coli methionine aminopeptidase from the structural analysis of reaction products and phosphorus-based transition-state analogues. *Biochemistry* **1999**, *38*, 14810−14819.
(39) Douangamath, A.; Dale, G. E.; D'Arcy, A.; Almstetter, M.; Eckl, R.; Frutos-Hoener, A.; Henkel, B.; Illgen, K.; Nerdinger, S.; Schulz, H.; Mac, Sweeney, A.; Thormann, M.; Treml, A.; Pierau, S.; Wadman, S.; Oefner, C. Crystal structures of Staphylococcusaureus methionine aminopeptidase complexed with keto heterocycle and aminoketone inhibitors reveal the formation of a tetrahedral intermediate. *J. Med. Chem.* **2004**, *47*, 1325−1328.
(40) Hu, X.; Addlagatta, A.; Matthews, B. W.; Liu, J. O. Identification of pyridinylpyrimidines as inhibitors of human methionine aminopeptidases. *Angew. Chem., Int. Ed.* **2006**, *45*, 3772−3775.
(41) Outten, C. E.; O'Halloran, T. V. Femtomolar sensitivity of metalloregulatory proteins controlling zinc homeostasis. *Science* **2001**, *292*, 2488−2492.

JM700930K